

Nitrogen doped ZrO₂ thin films: synthesis and characterization

V. Ciupina^{a,b,d}, M. Albu^a, A. Caraiane^a, C. Porosnicu^c, C. Staicu^{b,c}, V. Nicolescu^e,
R. Manu^{b,f,*}

^aOvidius University of Constanta, 124 Mamaia Ave., 900527, Constanta, Romania

^bFaculty of Physics, The University of Bucharest, 405 Atomistilor St., PO Box MG-11, RO – 077125, Magurele, Ilfov, Romania.

^cNational Institute for Laser, Plasma and Radiation Physics, 409C Atomistilor St., PO Box MG-36, 077125, Magurele, Ilfov, Romania

^dAcademy of Romanian Scientists, Splaiul Independentei St, No. 54, 050094, Bucharest, Romania

^eCERONAV, 69A Pescarilor St., 900581, Constanta, Romania;

^fNational Institute for Marine Research and Development “Grigore Antipa” 300 Mamaia Avenue, Constanta, Romania 90058

To obtain ZrO₂ and ZrO₂+N₂ thin films was used magnetron sputtering in radio frequency mode in a 10⁻⁶ mbar high vacuum deposition chamber. Silicon and carbon substrates measuring 12x15mm were used for deposition. The used magnetron system was composed of a single water-cooled cathode, provided with one circular targets of ZrO₂ (2 mm thick and 50 mm in diameter) of high purity (99.95%). TDS Analysis of the films was performed. The desorbed species were observed with a QMG 220 Mass spectrometer provided with a W filament. It can be observed that in the case of the ZnO₂ film, nitrogen desorption registers two maxima with signal intensity of 9.7x10⁻¹² and 9.0x10⁻¹², reached after 2000s and 4900s respectively. In the case of ZrO₂+N₂ film, nitrogen desorption shows a pronounced maximum with a signal intensity of 2.4x10⁻¹¹ reached after 6000s. . The topology the ZrO₂ and ZrO₂+N₂ samples deposited on Si substrates have been investigated by scanning electron microscopy (SEM) using a FEI Inspect S scanning electron microscope (Hillsboro, Oregon, OR, USA) in high-vacuum modes. For the ZrO₂ deposition, the surface appears to have grain-like topology, with a mean dimension of around 150 nm. These structures do not appear for the ZrO₂+N₂ deposition. Instead, for the ZrO₂+N₂ sample, small blisters (between 300 nm and 1.000nm) have formed on the surface, as a consequence of injecting N₂ during the deposition. Cross-section measurements were also performed to establish the layer thickness. The ZrO₂ sample has a measured thickness of 1950nm, while the introduction of N₂ gas for the ZrO₂+N₂ sample had a poisoning effect on the magnetron target that led to a decrease (5 times) in deposition rate, giving this sample a final thickness of 365nm (compared to 1950nm) for the same deposition. The crystalline structure was investigated using X-Ray Diffraction (XRD) method. The experimental set-up was composed of a diffractometer equipped with a Cu-K α X-ray source, with a specific wavelength of 0.154nm, in a Bragg-Bretano type geometry. In this way, a crystalline phase corresponding to ZrO₂ with a group symmetry Fm-3m (225)-face centered cubic was identified. At the same time, it is observed that the films deposited in the reactive atmosphere show a pronounced amorphization, this most likely being due to the retention of nitrogen which leads to the modification of the network parameters.

(Received August 22, 2022; Accepted November 11, 2022)

Keywords: ZrO₂, ZrO₂+N₂, Magnetron sputtering, TDS, SEM, XRD

1. Introduction

ZrO₂ is a very stable material. It has a high melting point (2983 K) and a total vapor pressure of 0.01 Pa at 2273 K. It is chemically quite inert; Pure zirconia (ZrO₂) has a monoclinic

* Corresponding author: rmanu@alpha.rmri.ro
<https://doi.org/10.15251/JOR.2022.186.759>

crystal structure at room temperature and tetragonal and cubic crystal structures at higher temperatures. The transition from tetragonal to monoclinic during cooling involves a large volume change and concomitant cracking and thus needs to be avoided. ZrO_2 can be stabilized in the tetragonal/cubic form by adding small amounts of other oxides such as MgO , Y_2O_3 , CaO , Ce_2O_3 , and also PuO_2 . Zirconium oxide (ZrO_2) is an attractive material in many fields because of its excellent mechanical, thermal optical, and electrical characteristics ([1],[2]). ZrO_2 can present three polymorphic crystalline structures, that is, monoclinic (below $1170^\circ C$), tetragonal ($1170\text{--}2370^\circ C$), and cubic (above $2370^\circ C$). Amorphous zirconia (ZrO_2) and zirconia-silica ($ZrO_2\text{--}SiO_2$) thin films on glass and silicon substrates were obtained by magnetron sputtering ([3]); based on zirconia-silica targets consisting by mixing ZrO_2 and SiO_2 in volume ratio were deposited films with important mechanical performance. The addition of SiO_2 lowered the internal stress of pure ZrO_2 films and also increased the resistivity and breakdown field and lowered the dielectric loss tangent of pure ZrO_2 films.

Optical properties, e.g. refractive index and optical transmittance, revealed that zirconium silicate films still remained highly transparent. Recently, there were many efforts devoted to fabricate $ZrO_2\text{--}CNT$ nanocomposites in hopes of broadening the applications of ZrO_2 ([4]–[9]). So, $ZrO_2\text{--}CNT$ nanocomposite prepared by a hydrothermal method was found to be a good biocompatible matrix for protein immobilization ([4]). In addition, it was also found that the Pt catalyst supported by $ZrO_2\text{--}CNT$ nanocomposites exhibited significantly improved catalytic activity toward methanol and ethanol oxidation in direct methanol and ethanol fuel cells compared with that supported by either CNTs or commercial C. Moreover, CNT transistors integrated with high-k ZrO_2 were applied as advanced gate dielectrics for future molecular electronics, which will be crucial. Thus, $ZrO_2\text{--}CNT$ nanocomposites are promising for applications in fuel cells, batteries, electronics devices, and chemical sensors. To fulfill these applications, it is of great importance to controllably synthesize $ZrO_2\text{--}CNT$ nanocomposites. In previous studies, the fabrication of $ZrO_2\text{--}CNT$ nanocomposites was mainly achieved by solution-based methods ([8]–[10]). In this respect, Sun et al. ([8]) synthesized $ZrO_2\text{--}CNT$ nanocomposites via decomposition of $Zr(NO_3)_4 \cdot 8H_2O$ in supercritical carbon dioxide-ethanol solution with dispersed CNTs at relatively low temperatures. Most of these studies were focused on controlling the phase ([2],[9],[10],[11]) or morphology of ZrO_2 coated on CNTs, and the CNTs used in these studies required a pretreatment process by either covalent ([11]) or noncovalent ([12],[13]) methods to functionalize their inert surface.

Zirconia dental implants are groundbreaking addition to the dental industry, being only viable option for a patient wishing to have dental implants but is concerned about metal-free dentistry. This material is inert and can be a good choice for people with known metal or sensitivities. Zirconia implants may be more aesthetically pleasing, eliminating the risk of dark lines around the gingival margin, especially when a one-piece zirconia implant is selected. Zirconia has good flexural strength and is known to be superior to other ceramics in resistance to fracture. Its white color, low modulus of elasticity, and low thermal conductivity have made this material a desirable choice for implant dentistry. Clinical studies have shown zirconia to be as good or even better than titanium in terms of osseointegration. (14).

2. Experimental set-up

The method used to obtain ZrO_2 and ZrO_2+N_2 thin films is magnetron sputtering. Prior to the actual deposits, some calibrations were performed to determine the materials deposition rate for reaching the desired thickness. ZrO_2 and ZrO_2+N_2 composite depositions were made using magnetron sputtering in radio frequency mode for ZrO_2 in a 10^{-6} mbar high vacuum deposition chamber (Fig.1).

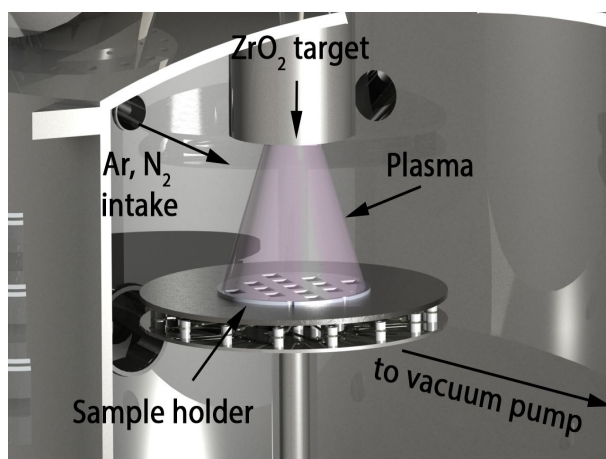


Fig. 1. Experimental set-up.

Silicon and carbon substrates measuring 12x15mm were used for deposition. They were ultrasonically cleaned in a mixture of isopropyl alcohol and acetone to remove impurities. The substrates were mounted in the vacuum chamber on a fixed circular holder placed at a distance of 10 cm from the sputtering source. The used magnetron system was composed of a single water-cooled cathode, provided with one circular targets of ZrO_2 (2 mm thick and 50 mm in diameter) of high purity (99.95%). The enclosure was degassed until the pressure reached 10^{-6} mbar. To clean the targets of oxides and other impurities, an argon discharge plasma was ignited. Throughout the cleaning process, the sample holder was shielded from the plasma with a shutter. During the deposits the working pressure was maintained at 2×10^{-2} mbar.

The deposition parameters, such as ZrO_2 radio frequency power P (W), working pressure (mbar), the gas flow (sccm) and deposition time are presented in Table 1.

Table 1.. Main deposition parameters for the ZrO_2 and ZrO_2+N_2 .

Film	P (W)	p (mbar)	Ar flux(sccm)	N_2 flux (sccm)	time
ZrO_2	80	1×10^{-2}	20	-	18h 20 min
ZrO_2+N_2	80	1×10^{-2}	20	20	18h 20 min

3. Results and discussions

3.1. Thermal Desorption Spectroscopy (TDS) analysis

Fig.2. shows a schematic of the TDS set-up. The desorbed species were observed with a QMG 220 Mass spectrometer provided with a W filament. The measurements started at a base pressure of $4 \cdot 10^{-6}$ Pa. For each measurement a sample was transported to the right end of the quartz tube with the help of a magnet after which the oven was positioned on the quartz tube so as to the sample to be in the center of the oven. The oven was provided with an in-built thermocouple placed in its center to accurately measure the temperature. The heating power supply was controlled with a Eurotherm proportional-integral deriver which automatically adjusted the percentage of power applied in order to maintain a stable heating rate. The oven was programmed to maintain a stable temperature of $1050^\circ C$ until the desired gas signal quenched.

Equipment: Mass Spectrometer - Quadera QMG 220; W filament Linear Heating Ramp: 10 K/min (final prograded temperature: 1320 K).

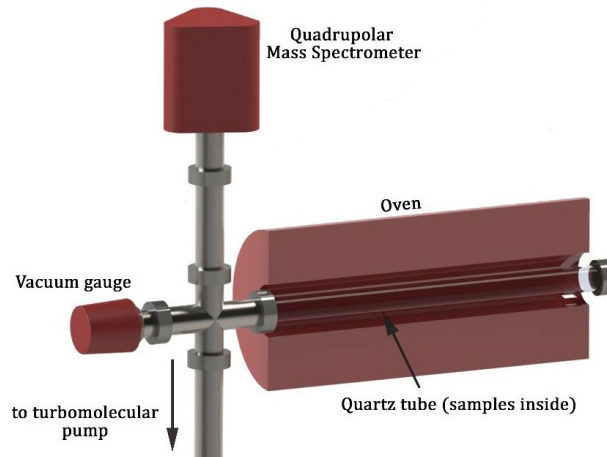


Fig.2. Schematic of the TDS set-up

In Figs.3,4,5 are plotted the graphs which represent the desorption signal of N_2 and O_2 and the temperature as a function of time. In Fig.3 are presented N_2 desorption curves for ZrO_2 layer (left hand) and O_2 desorption curves for ZrO_2 layers (right hand).

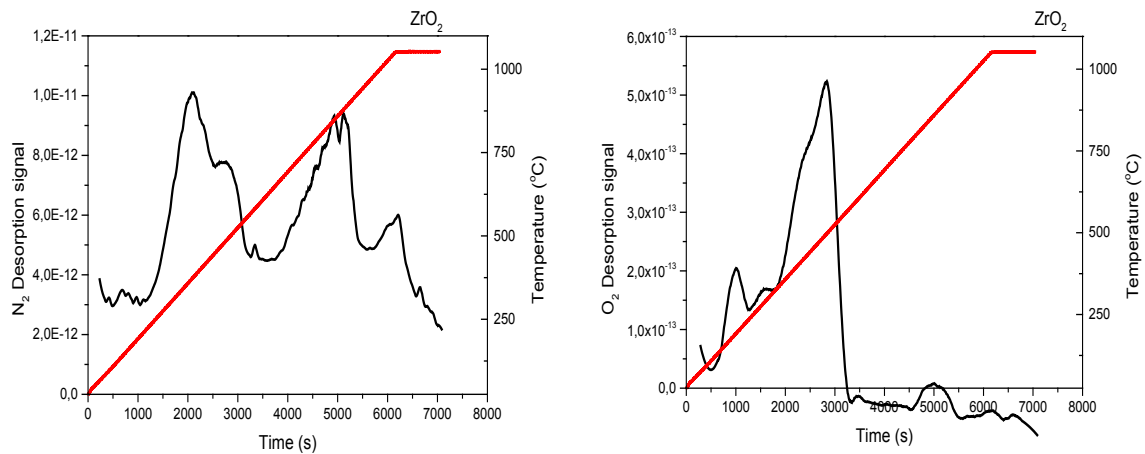


Fig. 3. N_2 desorption curves for ZrO_2 layer (left hand) and O_2 desorption curves for ZrO_2 layers (right hand).

In Fig.4 are shown the desorption curves in the case of ZrO_2+N_2 layers, i.e.: N_2 desorption curves for ZrO_2+N_2 layers (left hand), O_2 desorption curves for ZrO_2+N_2 layers (right hand).

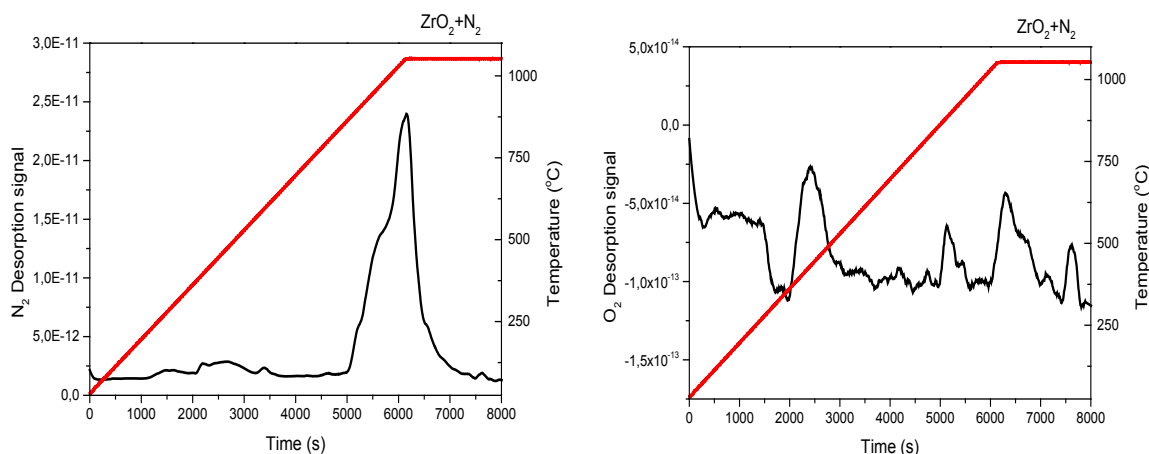


Fig. 4. Desorption curves in the case of ZrO_2+N_2 layers, i.e.: N_2 desorption curves for ZrO_2+N_2 layers (left hand), O_2 desorption curves for ZrO_2+N_2 layers (right hand).

For a better comparison, the graphs were condensed as it is described in Fig. 5.

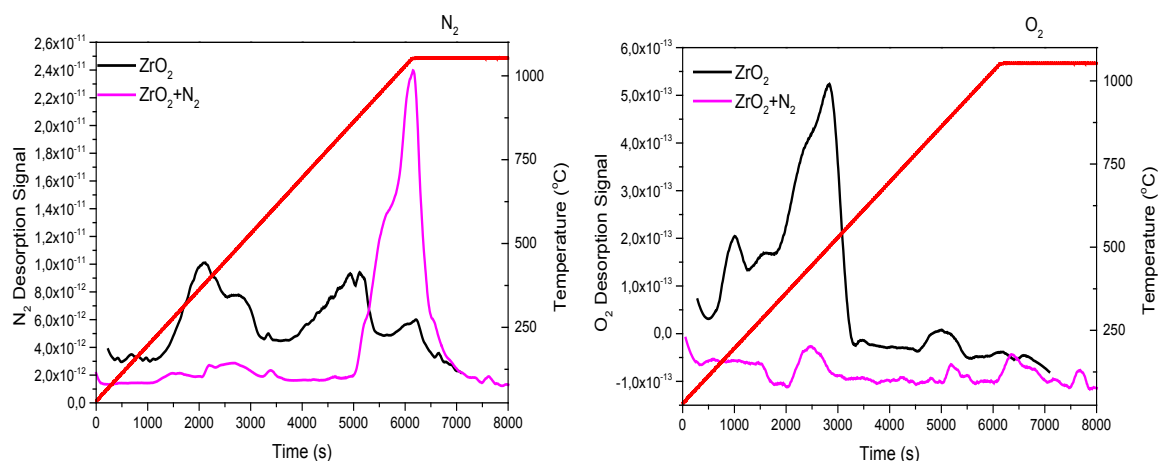


Fig. 5. Graphs condensed which described the curves for N_2 (left hand) and O_2 (right hand) desorption in the cases of ZrO_2 and ZrO_2+N_2 .

It can be observed that in the case of the ZnO_2 film, nitrogen desorption registers two maxima with signal intensity of 9.7×10^{-12} and 9.0×10^{-12} , reached after 2000s and 4900s respectively. In the case of ZrO_2+N_2 film, nitrogen desorption shows a pronounced maximum with a signal intensity of 2.4×10^{-11} reached after 6000s. Such a result was expected, highlighting the increase in the amount of nitrogen in the film as a result of nitrogen doping. Oxygen desorption in the case of the ZrO_2 film occurs with three maxima with signal intensity of 2.0×10^{-13} , 5.4×10^{-13} , and respectively 0.1×10^{-13} , reached after 1100s, 2700s and 5000s respectively. As for the ZrO_2+N_2 film, three maxima are evident with the signal intensity of -0.2×10^{-13} , -0.6×10^{-13} and respectively -0.1×10^{-13} , reached after 2500s, 5250s and respectively 6400s. It should be mentioned that the signal intensity of the maxima is over an order of magnitude higher in the case of nitrogen desorption than in the case of oxygen desorption.

3.2. Electron Microscopy studies (SEM).

The topology of the ZrO_2 and ZrO_2+N_2 samples deposited on Si substrates have been investigated by scanning electron microscopy (SEM) using a FEI Inspect S scanning electron microscope (Hillsboro, Oregon, OR, USA) in high-vacuum modes. Images at three magnifications

were taken (1.000x, 5.000x and 10.000x). For the ZrO_2 deposition, the surface appears to have grain-like topology, with a mean dimension of around 150 nm. These structures do not appear for the ZrO_2+N_2 deposition. Instead, for the ZrO_2+N_2 sample, small blisters (between 300 nm and 1.000nm) have formed on the surface, as a consequence of injecting N_2 during the deposition. Cross-section measurements were also performed to establish the layer thickness. The ZrO_2 sample has a measured thickness of 1950nm (Fig.6-left hand), while the introduction of N_2 gas for the ZrO_2+N_2 sample had a poisoning effect on the magnetron target that led to a decrease (5 times) in deposition rate, giving this sample a final thickness of 365nm (Fig.6-right hand) for the same deposition time.

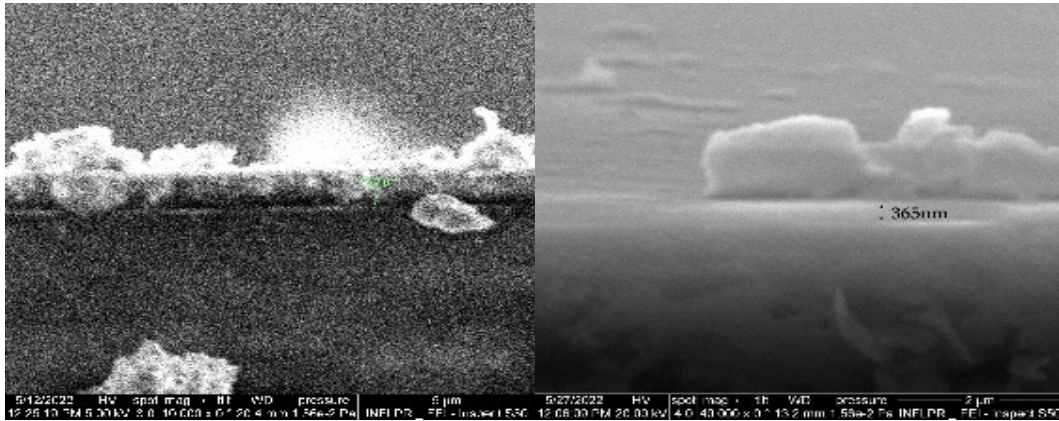


Fig. 6. Cross-section in the case of ZrO_2 sample (left hand) and ZrO_2+N_2 sample (right hand).

3.3. XRD characterizations

The crystalline structure was investigated using X-Ray Diffraction (XRD) method. The experimental set-up was composed of a diffractometer equipped with a $Cu-K\alpha$ X-ray source, with a specific wavelength of 0.154nm, in a Bragg-Bretano type geometry. The measured range was between 10^0-70^0 ; an incremental step of 0.02^0 and an integration time per step of 0.7s were used.

The images from Fig.7 and Fig.8 show the diffractograms corresponding to ZrO_2+N_2 and ZrO_2 thin films deposited by magnetron sputtering in RF mode. For the measurements, the face with largest flat surface available was used in order to obtain a better resolution by maximizing the number of scattering centers. The identification of the crystalline phases was achieved by comparing the position of the peaks in the diffractogram with the structure files in the Pearson database.

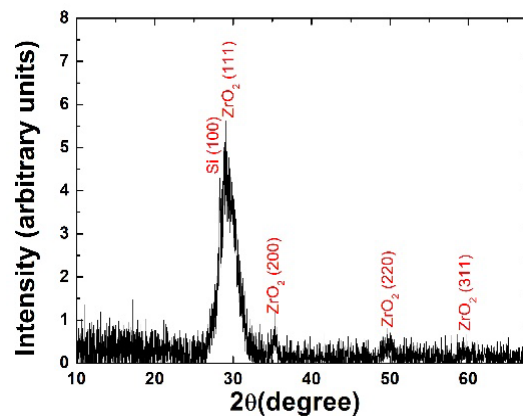


Fig. 7. XRD Zirconia + N_2 .

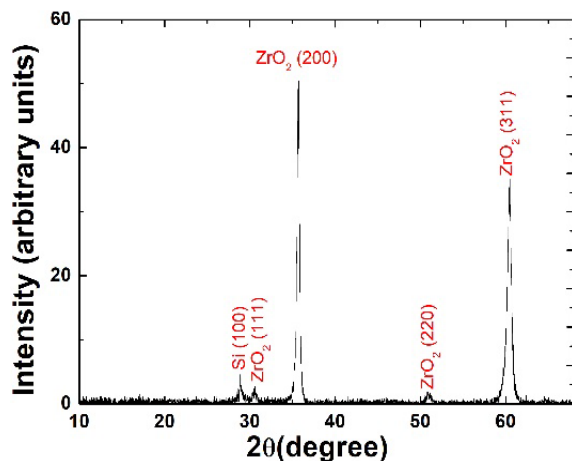


Fig. 8. XRD Zirconia.

In this way, a crystalline phase corresponding to ZrO_2 with a group symmetry Fm-3m (225)-face centered cubic was identified. The Miller indices corresponding to the main diffraction planes were (111), (200), (220) and (311), respectively.

For the ZrO_2 film deposited in the reactive nitrogen atmosphere ($Ar+N_2$), the crystallization mode is similar to that observed in the structure sheets, with a preferential growth of the crystallites on the (111) orientation. On the other hand, the ZrO_2 film deposited in the argon atmosphere shows preferential growth on (200) and (311) respectively. At the same time, it is observed that the films deposited in the reactive atmosphere (Fig.7) show a pronounced amorphization, this most likely being due to the retention of nitrogen which leads to the modification of the network parameters.

In Fig.9 is presented the diffractogram of the ZrO_2 sample. For the measurements, the face with the largest flat surface available was used in order to obtain a better resolution by maximizing the number of scattering centers. he crystalline.

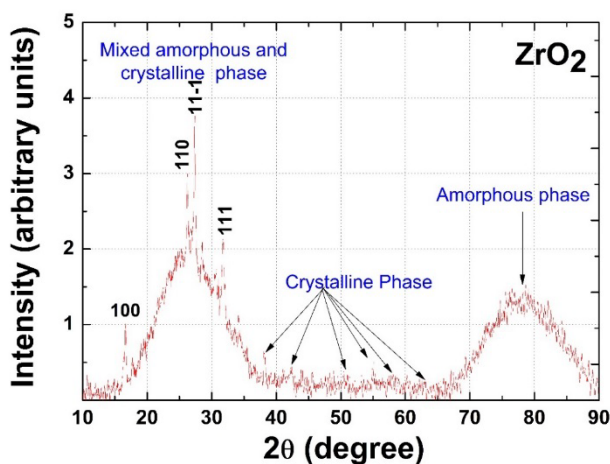


Fig. 9. The diffractogram of the ZrO_2 sample.

Three well-defined areas can be observed in the diffractogram. A first mixed area with a high degree of amorphization combined with the most intense orientations of the measured material, an area with a multitude of crystalline orientations of low intensity (the resolution of the equipment is not high enough to highlight them), and an area completely amorphized. The identification of the crystalline phases was achieved by comparing the position of the peaks in the

diffractogram with the structure files in the Pearson database. The only crystalline phase identified corresponds to the mineral 'baddeleyte' which is a rare form of ZrO_2 found in nature. It has a $P121/c1$ group symmetry with four ZrO_2 atoms in the unit cell. The 'baddeleyte' structure is a combination of tetrahedrally arranged oxide ions with the (100) plane and triangularly arranged ions. The main orientations observed in the measurement range are 100, 110, 11-1, 111, the mode of crystallization and the relative intensities of the orientations being similar to those observed in the structure sheets, the preferential crystallization plane being 11-1. Besides these, several peaks of low intensity are highlighted on the diffractogram. It should be mentioned that the number of crystallization planes in the measured reference interval is 118 (without excluding the double reflection planes and the prohibited ones). Considering the application of the material in dentistry, the 2 wide amorphous strips could correspond to the adhesive used to attach the veneer to the tooth.

4. Conclusions

To obtain ZrO_2 and ZrO_2+N_2 thin films was used magnetron sputtering in radio frequency mode in a 10^{-6} mbar high vacuum deposition chamber Silicon and carbon substrates measuring 12×15 mm were used for deposition. The used magnetron system was composed of a single water-cooled cathode, provided with one circular targets of ZrO_2 (2 mm thick and 50 mm in diameter) of high purity (99.95%).

TDS Analysis of the films was performed. It can be observed that in the case of the ZnO_2 film, nitrogen desorption registers two maxima with signal intensity of 9.7×10^{-12} and 9.0×10^{-12} , reached after 2000s and 4900s respectively. In the case of ZrO_2+N_2 film, nitrogen desorption shows a pronounced maximum with a signal intensity of 2.4×10^{-11} reached after 6000s. Such a result was expected, highlighting the increase in the amount of nitrogen in the film as a result of nitrogen doping. Oxygen desorption in the case of the ZrO_2 film occurs with three maxima with signal intensity of 2.0×10^{-13} , 5.4×10^{-13} , and respectively 0.1×10^{-13} , reached after 1100s, 2700s and 5000s respectively. As for the ZrO_2+N_2 film, three maxima are evident with the signal intensity of -0.2×10^{-13} , -0.6×10^{-13} and respectively -0.1×10^{-13} , reached after 2500s, 5250s and respectively 6400s. It should be mentioned that the signal intensity of the maxima is over an order of magnitude higher in the case of nitrogen desorption than in the case of oxygen desorption.

The topology of the ZrO_2 and ZrO_2+N_2 samples deposited on Si substrates have been investigated by SEM technology. For the ZrO_2 deposition, the surface appears to have grain-like topology, with a mean dimension of around 150 nm. For the ZrO_2+N_2 sample, small blisters (between 300 nm and 1.000nm) have formed on the surface, as a consequence of injecting N_2 during the deposition. Cross-section measurements were also performed to establish the layer thickness. The ZrO_2 sample has a measured thickness of 1950nm, while the introduction of N_2 gas for the ZrO_2+N_2 sample had a poisoning effect on the magnetron target that led to a decrease (5 times) in deposition rate, giving this sample a final thickness of 365nm for the same deposition time

The crystalline structure was investigated using X-Ray Diffraction method. A crystalline phase corresponding to ZrO_2 with a group symmetry $Fm-3m$ (225)-face centered cubic was identified. The Miller indices corresponding to the main diffraction planes were (111), (200), (220) and (311), respectively. For the ZrO_2 film deposited in the reactive nitrogen atmosphere ($Ar+N_2$), the crystallization mode is similar to that observed in the structure sheets, with a preferential growth of the crystallites on the (111) orientation. On the other hand, the ZrO_2 film deposited in the argon atmosphere shows preferential growth on (200) and (311) respectively. At the same time, it is observed that the films deposited in the reactive atmosphere show a pronounced amorphization, this most likely being due to the retention of nitrogen which leads to the modification of the network parameters. Based on the diffractogram of the ZrO_2 sample, three well-defined areas can be observed. A first mixed area with a high degree of amorphization combined with the most intense orientations of the measured material, an area with a multitude of crystalline orientations of low intensity and an area completely amorphized. The only crystalline phase identified corresponds to the mineral 'baddeleyte' which is a rare form of ZrO_2 found in

nature. The main orientations observed in the measurement range are 100, 110, 11-1, 111, the mode of crystallization and the relative intensities of the orientations being similar to those observed in the structure sheets, the preferential crystallization plane being 11-1. Besides these, several peaks of low intensity are highlighted on the diffractogram. Considering the application of the material in dentistry, the 2 wide amorphous strips could correspond to the adhesive used to attach the veneer to the tooth.

References

- [1] Lu, J.; Zang, J. B.; Shan, S. X.; Huang, H.; Wang, Y. H. *Nano Lett.* 2008, 8, 4070–4074; <https://doi.org/10.1021/nl801841r>
- [2] Luo, T. Y.; Liang, T. X.; Li, C. S. *Mater. Sci. Eng., A* 2004, 366, 206–209; <https://doi.org/10.1016/j.msea.2003.09.053>
- [3] D.H Kuo, C.H Chien, C.H Huang, *Thin Solid Films*, Volumes 420-421, 2 December 2002, Pages 47-53; [https://doi.org/10.1016/S0040-6090\(02\)00738-1](https://doi.org/10.1016/S0040-6090(02)00738-1)
- [4] Liang, R.; Deng, M.; Cui, S.; Chen, H.; Qiu, J. *Mater. Res. Bull.* 2010, 45, 1855–1860; <https://doi.org/10.1016/j.materresbull.2010.09.016>
- [5] Song, H.; Qiu, X.; Li, F. *Appl. Catal., A* 2009, 364, 1–7; <https://doi.org/10.1016/j.apcata.2009.04.046>
- [6] Guo, D.; Qiu, X.; Zhu, W.; Chen, L. *Appl. Catal., B* 2009, 89, 597–601; <https://doi.org/10.1016/j.apcatb.2009.01.025>
- [7] Javey, A.; Kim, H.; Brink, M.; Wang, Q.; Ural, A.; Guo, J.; McIntyre, P.; Mceuen, P.; Lundstrom, M.; Dai, H. *Nature* 2002, 1, 241–246; <https://doi.org/10.1038/nmat769>
- [8]. Pal, K.; Kang, D. J.; Zhang, Z. X.; Kim, J. K. *Langmuir* 2010, 26, 3609–3614; <https://doi.org/10.1021/la903022j>
- [9] Sun, Z.; Zhang, X.; Na, N.; Liu, Z.; Han, B.; An, G. *J. Phys. Chem. B* 2006, 110, 13410–13414; <https://doi.org/10.1021/jp0616359>
- [10]. Shan, Y.; Gao, L. *Nanotechnology* 2005, 16, 625–630; <https://doi.org/10.1088/0957-4484/16/6/001>
- [11] Lupo, F.; Kamalakaran, R.; Scheu, C.; Grobert, N.; Ruhle, M. *Carbon* 2004, 42, 1995–1999; <https://doi.org/10.1016/j.carbon.2004.03.037>
- [12] Banerjee, S.; Hemraj-Benny, T.; Wong, S. S. *Adv. Mater.* 2005, 17, 17–29; <https://doi.org/10.1002/adma.200401340>
- [13] Lu, Y.; Bangsaruntip, S.; Wang, X.; Zhang, L.; Nishi, Y.; Dai, H. *J. Am. Chem. Soc.* 2006, 128, 3518–3519; <https://doi.org/10.1021/ja058836v>
- [14] Cionca, N, Müller, N, Mombelli, A. Two-piece-zirconia implants supporting all-ceramic crowns. A prospective clinical study. *Clin. Oral Impl. Res.* 26, 2015, 413–418, <https://doi.org/10.1111/clr.12370>